Kinetic Energy–Mass Distributions from the Fission of Nuclei Lighter than Radium*

F. Plasil,† D. S. Burnett,‡ H. C. Britt,§ and S. G. Thompson

Lawrence Radiation Laboratory, University of California, Berkeley, California

(Received 19 August 1965)

The distributions in masses and total kinetic energies of fission fragments from a number of elements ranging from erbium to bismuth have been measured. The nuclei undergoing fission were produced by bombarding a variety of targets with projectiles ranging from He^4 to O^{16}. The energies of coincident fission fragments were measured using solid-state counters. The energy data were transformed to give mass–total kinetic energy density-of-events distributions. These distributions were compared with those calculated from an approximate version of the liquid-drop model which applies to this region of elements. General agreement in the shapes and widths of the distributions was found, particularly in the cases which involved small angular momenta and small nuclear temperatures. The dependence of the widths of the experimental distributions on the nuclear temperature was found to differ from that predicted by the theory, but uncertainties in the evaluation of nuclear temperatures for the reactions investigated may be large. Analysis of these uncertainties indicated that they were not large enough to alone account for the discrepancy, although this analysis was subject to some error. Angular momentum effects were studied by using certain combinations of targets and projectiles to give the compound nucleus Os^{186} at the same excitation energy but with different angular momenta. The effect of increasing angular momentum was to broaden and change the shape of the experimental distributions.

I. INTRODUCTION

ONE consequence of the complex nature of the fission process is that there exists, at present, no generally accepted and adequate theory that is capable of accounting for all observed effects. In recent years, however, considerable process has been made in the development of a theory of fission. Potential energy calculations[1,2] made in the framework of the liquid-drop model indicated that in the region of nuclei lighter than radium an important approximation could be made. This approximation, which depends on the assumption that the shapes of the "liquid-drop" nuclei at the saddle point can be considered as spheroids or a superposition of two spheroids, has made it possible for Nix and Swiatecki[3] to work out the implications of this simple, well-defined model in a systematic way from initial conditions to final observable distributions using standard methods of statics, dynamics, and statistical mechanics. In spite of the crude nature of a model that regards nuclei as drops of an incompressible uniformly charged liquid restricted to spheroidal shapes, the value of the approach becomes apparent when we remember that this is the first consistent attempt to reproduce the entire fission process through all its stages yielding from first principles calculated distributions, such as the mass-total kinetic energy distributions, that may be compared directly with measured distributions.

The purpose of this work is to provide data for nuclei of $A \lesssim 220$ where the Nix-Swiatecki theory is expected to apply, and to compare these results with the theoretical results. The restriction of the region of applicability to relatively light elements introduces an experimental problem, namely, that of small fission cross sections. There are, however, two effects which tend to increase fissionability and make such measurements feasible. These are: (a) high angular momenta such as are encountered in heavy ion reactions and (b) high excitation energies. The high angular momenta, while increasing the fissionability, introduced several complications. The most serious of these is that the Nix-Swiatecki theory, with which the results have been compared, has been developed only for the case of zero angular momentum. An attempt has been made to isolate the effects of angular momentum by comparing the results from the fission of the Os^{186} compound nucleus produced by $He^4 + W^{182}$ with that produced by $O^{16} + Er^{170}$ at the same excitation energy.

The high excitation energies required to induce fission do not complicate comparison of experimental and theoretical results. The theory covers the whole range of excitation energies encountered in this work and makes definite predictions concerning variations in the resulting fission distributions with nuclear temperature. In order to test these predictions, measurements have been made at several bombarding energies for each combination of target and projectile.

The projectiles used were O^{16} (from 102- to 165-MeV bombarding energy) and He^4 (from 40- to 120-MeV). Two distributions from C^{12} bombardments were also measured. The range of targets extended from Er^{170} to Bi^{209}. In all cases the energies of pairs of fission fragments from the same fission event have been measured

[1] S. Cohen and W. J. Swiatecki, Ann. Phys. (N. Y.) **22**, 406 (1963).

[2] V. M. Strutinskii, N. Ya. Lyashchenko, and N. A. Popov, Zh. Eksperim. i Teor. Fiz. **43**, 584 (1963) [English transl.: Soviet Phys.—JETP **16**, 418 (1963)]; and Nucl. Phys. **46**, 639 (1963).

[3] J. R. Nix and W. J. Swiatecki, Nucl. Phys. **71**, 1 (1965).

with semiconductor detectors and recorded in a correlated manner. The resulting energy versus energy distributions have been converted to mass versus total kinetic energy distributions. These, in turn, have been compared directly with similar distributions calculated from the Nix-Swiatecki theory.

II. EXPERIMENTAL

The experimental techniques and the methods of data processing were in many ways similar to those of Haines and Thompson[4] and have been described in detail in earlier reports.[5-7] A beam of alpha particles or heavy ions defined by two or more circular collimators of 2 mm diameter and up to 18 in. apart struck a thin target at the center of a circular fission chamber. Two collimated semiconductor detectors were mounted on radial arms inside the chamber. One of the detectors subtended an angle of 3–4° at the center of the chamber and was placed typically at 60° with respect to the beam direction. This choice was made because the angle subtended allowed a reasonable counting rate and yet defined the detector position sufficiently well to make insignificant the dispersions resulting from angular uncertainty. While one angle had to be defined in this way to satisfy a condition imposed by center-of-mass transformations,[5] the other detector subtended an angle of 15 to 20° which was large enough to collect all fission fragments in coincidence with the first detector.[6] The angular position of this large detector was typically 90° with respect to the beam direction, its exact position being determined for each bombardment by making a rough angular correlation measurement. Permanent magnets were placed in front of the two detectors to eliminate interference from low-energy electrons. Heavy ion beams of 10.3 ± 0.1 MeV per nucleon were obtained from the Berkeley Heavy Ion Linear Accelerator (Hilac). Aluminum foils were used to degrade the beam to the energy needed. Range-energy curves of Northcliffe[8] were used for this purpose. Helium ion beams were obtained from the Berkeley variable frequency 88 in. cylotron. In this case energy degradation was not necessary since the accelerator produced particles of the required energies directly. The beam currents used were less than 20 millimicroamperes (mμA) in the heavy-ion bombardments and up to 100 mμA in the cyclotron bombardments. The difference is due to the low duty cycle of the Hilac and the larger energy deposition of the scattered heavy ions in the depletion layer of the detector, which combined to

decrease the energy resolution substantially at beam levels above 20 mμA.

The following tagets were used in this study: Er^{170}, Yb^{174}, W^{182}, Au^{197}, and Bi^{209}. The erbium-, ytterbium-, and tungsten-enriched (90–99%) isotopes were obtained in oxide form from the Oak Ridge National Laboratory, converted to fluoride by precipitation from nitric acid solution and evaporated from a molybdenum crucible by means of electron bombardment into thin Ni foils. The commercial Ni foils had nominal thicknesses of 90 to 135 μg cm^{-2}. The gold and bismuth targets were also prepared by evaporation, but were self-supporting, with the exception of those used in experiments 1 and 6 of Table I, ranging in weight from 100 to 200 μg cm^{-2}. The data were corrected for the finite target thickness by using the relationship $\Delta E_t = cE^{1/3}$, where E is the fragment energy, c is a constant, and ΔE_t is the loss of energy due to target thickness. This relationship is based on the work of Alexander and Gazdik.[9] The constant c was determined for any particular target by measuring fission distributions at several values of the angle between the detector and the target plane. Errors from this source in the final energy spectra may have been as high as 0.8 MeV for the most unfavorable cases.

Several types of detectors have been used in this work, all with similar response characteristics and resolution. Gold surface-barrier silicon detectors with 150 Ω-cm resistivity were used in the heavy-ion-induced experiments. They were operated at a reverse bias of 10–15 V. At this bias all fission fragments are stopped in the depletion layer of the detector, but the scattered heavy ions, which cause an undesirable background of pulses, do not deposit all of their energy. In the cyclotron experiments phosphorus-diffused semiconductor detectors of 200–400 Ω-cm resistivity were typically used. They were operated at a bias of 100–150 V. In this mode of operation both types of detectors showed good energy resolution as measured with fission fragments from the spontaneous fission of Cf^{252} before and after each experiment. The detectors were supplied by W. Hansen of this laboratory. The leakage current in the detectors was continuously monitored during each run. It was found to increase rapidly when radiation damage became appreciable. This was sometimes found to be the case during bombardments with heavy ions over a long period of time. Detectors with currents greater than 3 μA were always replaced. The calibration of the detectors will be discussed in the next section.

The electronic equipment consisted of two linear amplification systems, a fast and slow coincidence system, and a multiparameter pulse-height analyzer with a magnetic tape recording unit. The analyzer used during the heavy-ion experiments was locally built, and that during the cyclotron experiments (with one exception mentioned in Sec. IV) was a Nuclear Data analyzer,

[4] E. L. Haines and S. G. Thompson, Phys. Rev. **131**, 2169 (1963).

[5] E. L. Haines, Ph.D. thesis, Lawrence Radiation Laboratory Report UCRL-10342, 1962 (unpublished).

[6] D. S. Burnett, Ph.D. thesis, Lawrence Radiation Laboratory Report UCRL-11006, 1963 (unpublished).

[7] F. Plasil, Ph.D. thesis, Lawrence Radiation Laboratory Report UCRL-11193, 1963 (unpublished).

[8] L. C. Northcliffe, Phys. Rev. **120**, 1744 (1960).

[9] J. M. Alexander and M. F. Gazdik, Phys. Rev. **120**, 874 (1960).

Table I. Experimental results and theoretical calculations for the moments of over-all distributions for all reactions studied. Experimental results corrected for prompt neutron effects are also given. The errors shown are estimates of systematic errors (see text). Statistical errors are small in comparison with systematic errors. Certain duplicated experiments are also shown. E_L and θ are the bombarding energy and the nuclear temperature at the saddle, respectively. $\langle E_T \rangle$ is the average total kinetic energy and $\mu_2(E_T)$ the variance of the over-all total kinetic energy-yield distributions. $\mu_2(A_1)$ is the variance of the over-all mass-yield distribution. The asterisk superscript characterizes values after the emission of prompt neutrons.

E_L (MeV)	θ (MeV)	Number of events (×10³)	Experiment order	Experiment $\langle E_T^* \rangle$ (MeV) uncorrected	$\langle E_T \rangle$ (MeV) corrected	Theory $\langle E_T \rangle$ (MeV)	Experiment $\mu_2(E_T^*)$ (MeV)² uncorrected	$\mu_2(E_T)$ (MeV)² corrected	Theory $\mu_2(E_T)$ (MeV)²	Experiment $\mu_2(A_1)$ (amu)² uncorrected	$\mu_2(A_1)$ (amu)² corrected	Theory $\mu_2(A_1)$ (amu)²
$Bi^{209}+He^4=At^{213}$												
120	1.87	197	7	141±3	148±4	149	102±6	78	108	197±7	169	209
120	1.87	202	9	144	152	149	108	83	108	191	163	209
100	1.66	94	7	140	147	150	95	78	95	185	165	186
100	1.66	152	9	143	150	150	101	83	95	179	159	186
80	1.42	163	8	143	148	150	95	84	81	168	156	160
80	1.42	200	9	143	148	150	95	84	81	165	152	160
65	1.21	101	1	146	150	150	81	74	68	141	131	135
60	1.12	235	8	144	147	150	85	78	63	142	135	126
40	0.71	57	8	144	146	150	67	65	40	97	94	80
$Au^{197}+He^4=Tl^{201}$												
120	1.95	132	7	136±3	143±4	141	91±6	67	105	190±6	166	226
120	1.95	88	9	136	143	141	97	74	105	196	172	226
100	1.74	71	9	135	141	141	90	73	93	180	162	203
80	1.49	88	8	135	140	141	88	78	79	168	157	175
80	1.49	74	9	135	140	141	85	74	79	162	151	175
70	1.36	43	6	138	142	142	78	69	72	146	137	159
60	1.20	51	8	135	138	142	76	70	63	139	132	140
$W^{182}+He^4=Os^{186}$												
120	2.00	145	7	122±3	128±4	130	86±6	68	101	220±7	204	256
100	1.77	85	7	121	125	130	81	67	88	211	200	229
$W^{182}+O^{16}=Pb^{198}$												
165	2.07	102	4	140±3	147±4	142	154±8	134	114	256±10	243	210
144	1.87	110	5	139	146	142	132	116	103	239	229	191
127	1.70	43	4	140	146	142	120	108	94	211	203	174
115	1.55	41	5	140	144	142	106	96	85	191	185	159
102	1.37	38	4	140	144	143	92	85	74	160	156	140
$Er^{170}+O^{16}=Os^{186}$												
165	2.04	152	2, 4, 5	120±4	127±5	130	124±10	106	104	250±14	235	261
151	1.91	27	2	121	128	130	111	96	95	227	215	246
136	1.73	70	2, 5	119	124	130	108	97	86	220	211	224
120	1.49	46	2, 4	119	124	131	97	89	73	205	199	193
$Yb^{174}+C^{12}=Os^{186}$												
125	1.70	31	3	125±4	129±5	130	115±12	104	84	217±16	211	222
109	1.53	21	3	123	127	131	102	94	76	190	185	197

model ND 160, with a buffer memory and tape unit.[10] The linear amplification system was maintained at a high level of stability. This stability was continuously monitored during each run by means of a high precision mercury pulse generator which fed pulses through the entire system. The maximum drift during any run was under 1%, and no corrections to the data were found to be necessary. The outputs of the two linear systems went directly to the multiparameter analyzer. The fast coincidence system was of such time resolution (about 20–30 nsec) as was required to eliminate accidental events, but gave an output pulse every time both fragments from a single event were detected. This output was delayed and fed into a slow coincidence unit, which also required the presence of the two linear pulses. The output of this unit activated the multiparameter analyzer in the case of the heavy-ion experiments, and it opened gates allowing the linear pulses to reach the analyzer in the cyclotron experiments. In the experiments at the Hilac, Model VI Goldsworthy[11] linear amplifiers and preamplifiers were used, together with several Hewlett-Packard distributed amplifiers and transistorized coincidence units. In the cyclotron experiments pulse-shaping, amplification, fast and slow

coincidence, and linear gating were all performed in one unit designed by Goulding and Landis.[12] Two dimensions of the multiparameter analyzer were used, one for each of the two fission fragments. The data were stored event by event on magnetic tape in such a way that pairs of pulse heights, corresponding to any one given fission event, were kept together. Thus the number of events $N(P_1, P_2)$ in which fragment 1 produced a pulse height P_1 and fragment 2 produced a pulse height P_2 was measured for all combinations of P_1 and P_2, resulting in a two-dimensional number-of-events distribution. The magnetic tapes were processed on IBM 7090 and 7094 computers.

The total number of events measured in any one distribution ranged from 2×10^4 to 2×10^5. In the case of heavy-ion reactions, very slow counting rates were encountered, making it sometimes necessary to add together data from several experiments. In the case of the cyclotron experiments, several distributions were remeasured at different times to check reproducibility and consistency. The reactions studied and the numbers of events recorded are given in Table I.

[10] Nuclear Data Inc., Palatine, Illinois.
[11] W. W. Goldsworthy, Lawrence Radiation Laboratory Report UCRL-9816, 1961 (unpublished).

[12] F. S. Goulding and D. Landis, in *Instrumentation Techniques in Nuclear Pulse Analysis* (National Academy of Sciences–National Research Council, Washington, D. C., 1963), Publication No. 1184.

III. CALCULATIONS

A. Calibration of Semiconductor Detectors

Several methods of calibration of semiconductor detectors have been considered during the course of this work.[6,7] The most successful method in the early stages of this study was one that takes advantage of the large center-of-mass effect in heavy-ion bombardments. Due to this effect, fission fragments at forward angles have a considerably higher kinetic energy than those at backward angles.[4,5] The fission spectrum resulting from the reaction $Bi^{209}+(165 \text{ MeV})O^{16}=Pa^{225}$ was measured at several angles. The average positions of these spectra defined the energy calibration for fragments of mass 112. The energy calibrations for other masses depended on the construction of lines parallel to the mass 112 line in an energy pulse-height diagram. The spacing of the lines was determined on the basis of the two peaks from spontaneous fission of Cf^{252}.[13,14]

In the later stages of this work, a comprehensive and consistent method of calibrating semiconductor devices became available from the extensive work of Schmitt, Kiker, and Williams.[15] Their method makes the intercept as well as the slope of calibration equations dependent on mass according to the equation

$$E=(a+a'M)x+b+b'M,$$

where E is the energy of the detected particle, M is its mass, x is the observed pulse height, and a, a', b, and b' are constants. The values of these constants are the same for all detectors of the type used by these authors, and the values quoted by them were used in this work. The method of calibration used in all the cyclotron work was identical to that suggested in Appendix B of Ref. 15. In the heavy-ion work the first method of calibration was used as described above, but a careful comparative study of the two methods showed them, for practical purposes, to give identical results (within 1.0% for all quantities of interest).

B. Transformations

While the primary data may be viewed as a density distribution of events in a pulse-height 1 versus pulse-height 2 plane, the above calibration together with a correction for the loss of energy of the fragments due to the finite thickness of the target transforms this distribution into one that has the two measured fragment energies as the new coordinates. By means of a center-of-mass correction[5] and a random number technique, the coordinates may be changed to E_1^* and E_2^* where the energies are now center-of-mass energies, and the asterisk identifies quantities measured

after the emission of neutrons. A further transformation made use of conservation of momentum in fission from which the expression $A_1/A_c=E_2/E_T$ may be derived. Here A_1 and A_c are the masses of fragment 1 and the compound nucleus, respectively, and E_2 and E_T are the energy of fragment 2 and the total kinetic energy of both fragments, respectively.

We replaced the above exact expression with the approximate relation:

$$A_1\cong(E_2^*A_c)/(E_1^*+E_2^*).$$

The error introduced by replacing pre-neutron emission energies with post-neutron emission energies is very small and is discussed fully in Ref. 7. The new coordinates of the measured distributions $P(E_T^*,A_1)$ are, thus, the mass (before neutron emission) of fragment 1, A_1, and the total kinetic energy (after neutron emission) released in the process (E_T^*).

C. Statistical Calculations

The measured distributions $P(E_T^*,A_1)$ have been analyzed in terms of their first and second moments. These have been calculated for the over-all distributions in one variable (e.g., mass-yield curves) as well as for the distributions in one independent variable taken as a function of the other variable (e.g., mass-yield curves for a set of E_T values). The first moment, $\mu_1(x)$ of a distribution in a variable x is the mean of the distribution $\langle x \rangle$. The second central moment is the variance $\mu_2(x)$ which is the measure of the width of the distribution[16] and is given by

$$\mu_2(x)=\langle x^2 \rangle-\langle x \rangle^2.$$

The fourth moment $\mu_4(x)$ was also calculated and used in estimating statistical standard errors in the second moments.

The distributions were not "folded," i.e., the symmetry of mass distributions has not been forced. This gave a valuable check on the data. Reference 6 discusses the symmetry properties that the distributions had to satisfy.

D. Neutron Emission Effects

The emission of neutrons has to be considered in two ways:

(a). Pre-fission neutron emission from the compound nucleus introduces an uncertainty in the excitation energy, and hence the nuclear temperature at the time of fission. A knowledge of the nuclear temperature is required for a comparison of experiment with theory, and this effect will be considered in Subsection E.

(b). The effect that neutron emission from the fragments has on the shape of the mass-total kinetic energy distributions $P(A_1,E_T)$, in general, and on the values of moments of these distributions, in particular, is of

[13] J. S. Fraser, J. C. D. Milton, H. R. Bowman, and S. G. Thompson, Can. J. Phys. **41**, 2080 (1963).

[14] S. L. Whetstone, Phys. Rev. **131**, 1232 (1963).

[15] H. W. Schmitt, W. E. Kiker, and C. W. Williams, Phys. Rev. **137**, B837 (1965).

[16] The full width at half-maximum, FWHM, is given for a Gaussian distribution, by: $\text{FWHM}=2.36\sqrt{\mu_2}$.

great importance since the theoretical distributions do not take neutron emission into account. Although for any given combination of values of A_1 and E_T there is a distribution in the numbers of neutrons ν_1 and ν_2 emitted from the two fragments, we have neglected this as well as any correlation of ν_1 and ν_2 with A_1 and E_T, i.e., we assume $\nu_1 = \nu_2 = \frac{1}{2}\nu_T$. The formulas used to correct the moments and to calculate ν_T, together with an outline of their derivation, are given in Appendix A. They are based on the method of Haines.[5] The most important correction is that made to the absolute magnitude of the total kinetic energy, E_T. The extent of this correction can be seen from the data tabulated in Table I. Neutron emission from the fragments also enters into the calculation of A_1 discussed earlier. Errors from this source are small since the approximation $E_1/E_T \approx E_1^*/E_T^*$ is a good one. It gives exact results for the case $\nu_1 = \nu_2$ and introduces a maximum error of only one or two mass units if ν_1 and ν_2 are very different.

The effect of neutrons on the widths of the over-all distributions (mass-yield and E_T-yield curves) is appreciable. Corrected and uncorrected results will be given. The effects of neutrons on variances of conditional distributions such as $\mu_2(A_1)$ and the variance of the mass distribution as a function of E_T are remarkably small. Uncorrected results will be presented. In the case of $\langle E_T \rangle$ considered as a function of mass, the only effect is in the absolute value of E_T, and corrected results will be given.

An alternative approach to the question of prompt neutron emission from fission fragments has also been explored. This method attempts to transform entire distributions rather than just the statistical moments. The main problem of such a transformation is that the manner in which the deformation energy at the saddle divides between the two fragments for every event considered must be known. This information, while at present unavailable experimentally, is a product of the Nix-Swiatecki theory. It is therefore possible to invert the problem and "fold in" neutron effects into the theoretical calculations. The theoretical calculations are thus made to take the exact form of the measured distributions (excluding only angular momentum effects). These calculations have been performed, for several cases, using a Monte Carlo technique. The method and results are given in Appendix B. The results compare favorably with those from the more conventional approach of Appendix A, and the discussion and conculsions in this work are unaffected by the choice of method of correction.

E. Theoretical

Mass-total kinetic energy probability distributions, which can be compared with the measured $P(A_1, E_T^*)$ density-of-events distributions, have been calculated directly from the theory of Nix and Swiatecki[3]. In this theory, which in its present state of development holds only for the case of zero (or low) angular momentum, the compound nucleus is considered to be an irrotational, uniformly charged liquid drop. Its shape is restricted to that of a spheroid or to two spheroids, which may be overlapping or tangent to each other. The potential energy surface was calculated by Nix and Swiatecki in this parametrization. Classical equations of motion were solved, allowing the liquid drop in an initial state of motion to be followed, in terms of its energy and deformation, through the scission and fragment separation processes to infinity. The assumption of statistical equilibrium at the saddle gave a distribution of initial conditions which was combined with the relationship between these conditions and final observable quantities to produce expressions for the mass-total kinetic energy probability distribution. The remarkable feature of this theory is that a simple model has been consistently followed through the entire fission process and that there are no adjustable parameters involved when comparisons with experiments are made. An important step in the development of the theory is the expansion of the potential energy about the saddle point. This expansion is required for the calculation of the probability distributions for initial conditions. When only harmonic terms are retained, quantum mechanically correct results may be obtained. These results are the most accurate available at very low nuclear temperatures. In this work, however, temperatures were relatively high so that classical statistical mechanics is valid for determining the initial conditions. Under these circumstances Nix and Swiatecki have found it possible to retain anharmonic terms in the potential energy expansion, and these were found to have a significant effect on the final calculated distributions.[3] The theoretical distributions used in this work include anharmonicity effects, in contrast to those used in Refs. 6 and 7. All theoretical curves shown in the figures were obtained by numerical means from the appropriate expression for $P(A_1, E_T)$ given in Ref. 3.

The widths of theoretical distributions are dependent on the nuclear temperature at the saddle point. As was indicated, pre-fission neutron emission complicates the calculation of the excitation energy, and hence also the calculations of the nuclear temperature. In the case of heavy-ion bombardments, calculations based on the analysis of measured excitation functions, however, indicated that the average number of pre-fission neutrons was relatively small (0.2–1.5).[7] These calculations are described in detail in Ref. 7, and will also be the subject of a later report. Only brief description is given here. Branching ratios between fission and neutron emission along the neutron evaporation chains were evaluated at many fixed values of angular momentum, using a modified version of the level width expressions given by Huizenga and Vandenbosch.[17] These branching ratios

[17] J. R. Huizenga and R. Vandenbosch, in *Nuclear Reactions*, edited by P. M. Endt and P. B. Smith (North-Holland Publishing Company, Amsterdam, 1962), Vol. II, p. 42.

involve the fission barrier and the level density parameters, which were both left adjustable, although the functional variation of the fission barrier with angular momentum was taken from the calculations of Cohen, Plasil, and Swiatecki.[18] Partial probabilities for fission at given values of angular momentum and at various stages of the neutron evaporation chain were evaluated by means of the branching ratios. These partial probabilities were integrated numerically over a classical angular momentum distribution and over the neutron evaporation chains, giving a total fission cross section. This calculated cross section was then fitted, together with other calculated cross sections at different excitation energies, to excitation functions of Sikkeland[19] by adjusting the variable parameters mentioned above. The calculations computed such quantities as the average number of pre-fission neutrons and the average excitation energy at the saddle. These results were used to calculate nuclear temperatures for the various heavy ion cases. A similar study was carried out for the case of $He^4 + Au^{197}$. The pre-fission neutron-emission effects were even smaller, and they were consequently neglected for all targets bombarded with helium ions.

It should be stressed that although the critical parameters of these calculations (the fission barrier and the level density parameters) are not well established for most cases studied, they were left adjustable, and thus the information required (number of neutrons evaporated before fission) was extracted essentially directly from experimental excitation functions. As was discussed in Ref. 7, however, the calculated cross sections did not give good fits to the entire experimental excitation function in several cases, within reasonable limits imposed on the adjustable parameters by their physical significance. The cause of this discrepancy is not understood. At the present time, therefore, the results must be considered as rough estimates of the number of pre-fission neutrons. This introduces an unknown uncertainty into the estimates of nuclear temperature, and a large number of pre-fission neutrons cannot be unambiguously ruled out.

The equation of state,

$$E_x{}^S = a\theta^2 - \theta ,$$

which relates the nuclear temperature at the saddle θ to the excitation energy at the saddle $E_x{}^S$ was used.[20] In this expression, a is the level density parameter, taken to be equal to $\frac{1}{8}A_c$. $E_x{}^S$ is given by

$$E_x{}^S = E_x - B_f ,$$

where E_x is the excitation energy of the compound

nucleus as calculated from Cameron's masses,[21] and B_f is the liquid-drop fission barrier[1,18] corrected for ground-state shell effects. In the heavy-ion induced fission, where use of the above neutron evaporation calculations has been made, $E_x{}^S$ was a quantity averaged over the angular momenta and the numbers of pre-fission neutrons involved. A tabulation of θ values is given in Table I.

IV. PRESENTATION OF EXPERIMENTAL RESULTS

The reactions studied, the total number of events measured, the nuclear temperatures at the saddle point, and the first and second moments of the over-all distributions, both corrected and uncorrected for neutrons, are tabulated in Table I. The order in which experiments were performed is also given. As can be seen, several experiments have been repeated at different times in an effort to establish reproducibility for small changes in experimental conditions (e.g., different detectors and amplifier gains). The error estimates given in the table have been obtained primarily from these duplicate measurements and from the scatter in the data when examined as a function of excitation energy. As was noted in Sec. II, some heavy-ion reactions involved such low counting rates that it was in some cases necessary to add together data from several runs. Variations between individual runs making up the total distributions were used to estimate the errors given in Table I for the heavy-ion-induced fission cases. In all cases errors due to counting statistics were very much smaller than systematic errors. An important point is that the data from fission of Bi^{209} induced with 65-MeV He^4 ions were obtained considerably earlier than the rest of the He^4 data.[6] Several changes in technique make this point an entirely independent experiment. (Instead of the equipment described in Sec. II, this experiment involved the use of a nickel-backed bismuth target, detectors of 1700 Ω-cm resistivity, Goldsworthy Model VI amplifiers, a slow coincidence instead of a fast-slow coincidence system, and a different multiparameter analyzer. Furthermore, the method of calibration was not that of Schmitt et al.,[15] but was based on the alpha particles as well as on the fission fragments from a Cf^{252} source.[6]) The 65-MeV data agree within the quoted limits with those obtained by interpolation from the later experiments. This is further evidence for the likelihood that the quoted errors are realistic estimates of the actual systematic errors and gives us some confidence in comparing the Hilac and cyclotron data taken under considerably different experimental conditions as discussed in Sec. II.

Six types of figures have been used to present the data. These consist of:

[18] S. Cohen, F. Plasil, and W. J. Swiatecki (to be published).
[19] T. Sikkeland, Phys. Rev. 135, B669 (1964).
[20] J. M. B. Lang and K. J. LeCouteur, Proc. Phys. Soc. (London), A67, 586 (1954). The value used for a was obtained from K. J. LeCouteur and D. W. Lang, Nucl. Phys. 13, 32 (1959).

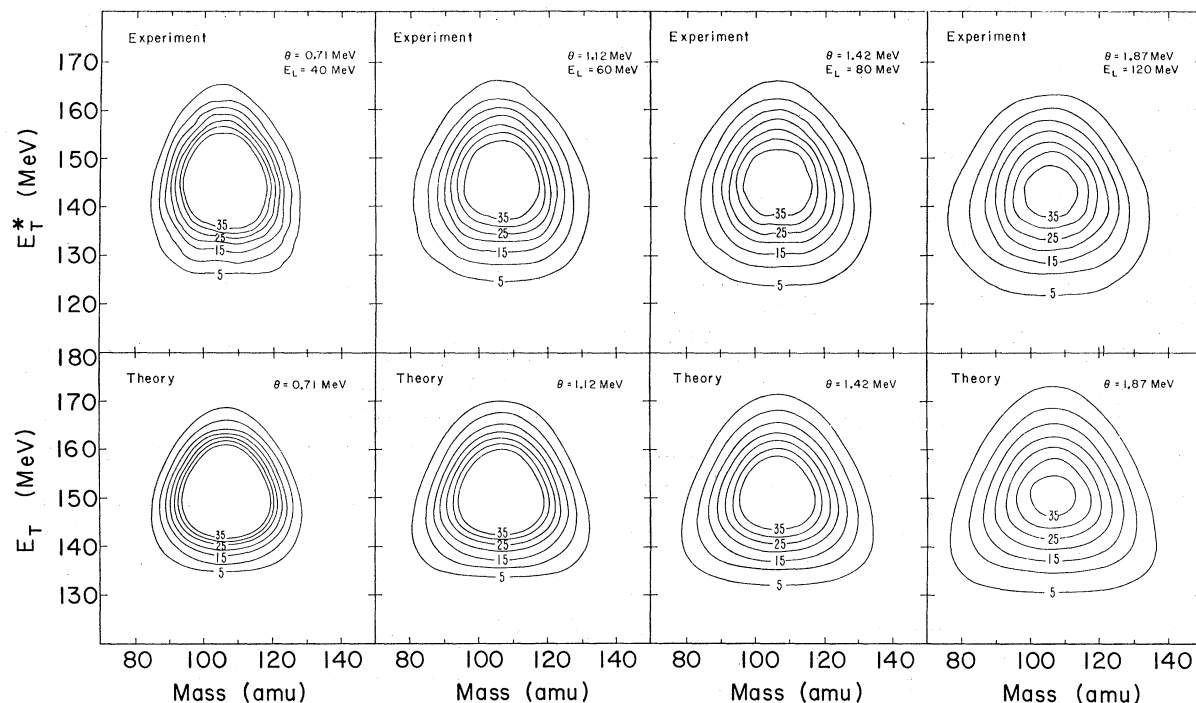[21] A. G. W. Cameron, Can. J. Phys. 35, 1021 (1957), and Chalk River Report CRP-690, 1957 (unpublished).

FIG. 1. Experimental and theoretical contour diagrams for the probability distributions, $P(E_T, A_1)$, of fragment total kinetic energy, E_T, and mass, A_1, for the reaction $He^4 + Bi^{209} = At^{213} \rightarrow$ fission. Several values of the nuclear temperature of the compound nucleus, θ, and corresponding laboratory bombarding energies, E_L, are shown. The labels on the lines of constant probability have the following significance: a contour labeled 10, for example, would pass through those regions of the E_T versus A_1 plane where an area of 6 MeV by 3 amu contains 1% of the total number of events. Seven contours are shown at all values of θ; higher contours are present in the case of narrow distributions at low θ values, but are not shown.
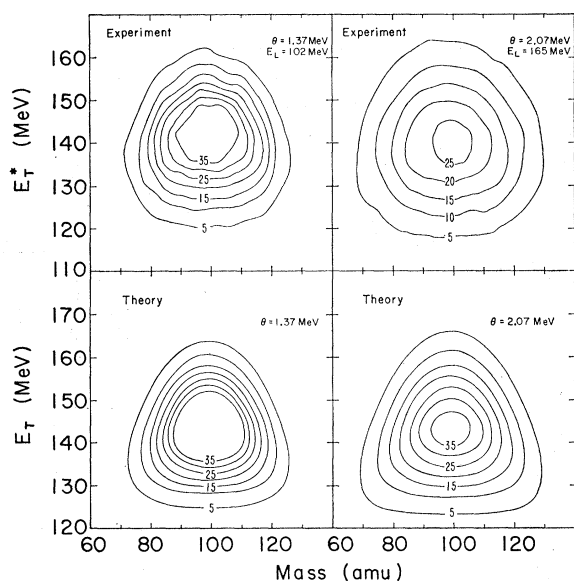
FIG. 2. Experimental and theoretical contour diagrams of the mass-total kinetic energy probability distributions for the fission of Pb^{198} produced by O^{16} bombardment of W^{182} at two values of the nuclear temperature, θ, and bombarding energy, E_L. The significance of contour labels is the same as that in Fig. 1.

(i). Mass-total kinetic energy contour diagrams (Figs. 1–3).

(ii). Over-all distributions such as mass-yield and total kinetic energy-yield distributions (Figs. 4–7).

(iii). Variances of the over-all distributions as a function of nuclear temperature (Figs. 8–11).

(iv). The average total kinetic energy, $\langle E_T \rangle$, as a function of mass (Figs. 12–13).

(v). The variances of the total kinetic energy distributions, $\mu_2(E_T)$, as a function of mass (Figs. 14–15).

(vi). The variances of the mass distributions, $\mu_2(A_1)$, as a function of the total kinetic energy (Figs. 16–17).

With the exception of Figs. 8, 9, 12, and 13, the experimental results have not been corrected for neutron effects. In the case of Figs. 12 and 13, an uncorrected curve is essentially identical to that shown, except for an over-all decrease in magnitude of the entire experimental curve. The corrected curves of variances of conditional distributions (Figs. 14–17) are only slightly lower in magnitude than those presented in the figures.[6]

The most complete method of presenting a mass-total kinetic energy distribution is in the form of a contour diagram. Such diagrams are shown in Figs. 1–3. The contour lines pass through regions of constant density-of-events in the experimental case, and through
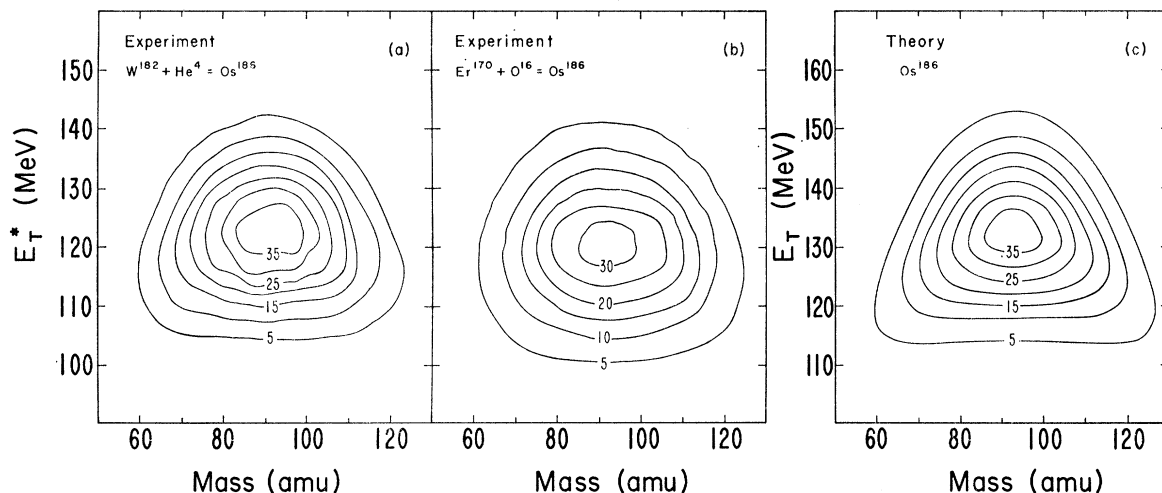
FIG. 3. Experimental and theoretical contour diagrams of the mass-total kinetic energy distributions for the fission of Os^{186} at a nuclear temperature of 2 MeV. The Os^{186} compound nucleus was produced by a He^4 bombardment (at 120 MeV) of W^{182} and by an O^{16} bombardment (at 165 MeV) of Er^{170}. The significance of contour labels is the same as that in Fig. 1.
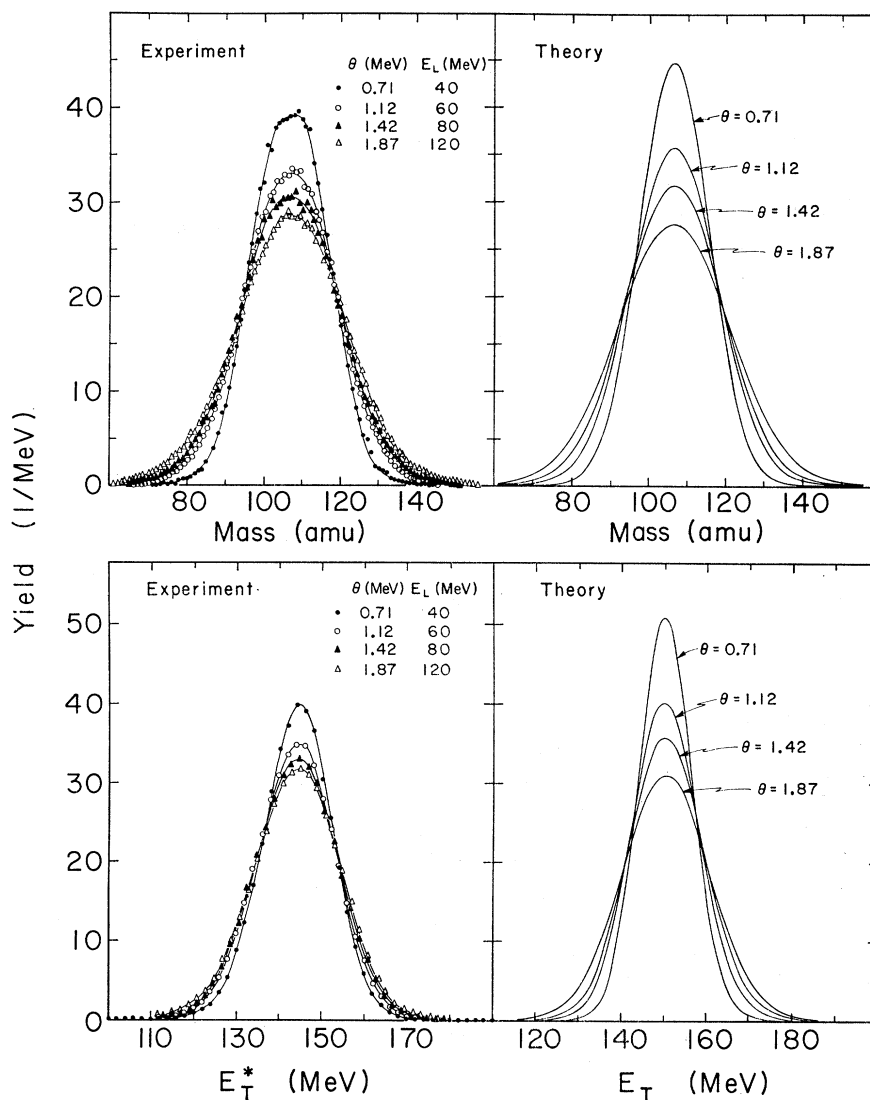
FIG. 4. Mass-yield and total kinetic energy-yield distributions (experimental and theoretical) for the fission of the At^{213} compound nucleus produced by He^4 bombardments of Bi^{209} at several bombarding energies. The units of yield are arbitrary. The E_T^* scale given is that for the $\theta=0.71$-MeV case. Other experimental energy-yield distributions shown were normalized in such a way as to make their average total kinetic energy $\langle E_T \rangle$, equal to $\langle E_T \rangle$ of the $\theta=0.71$-MeV distribution.
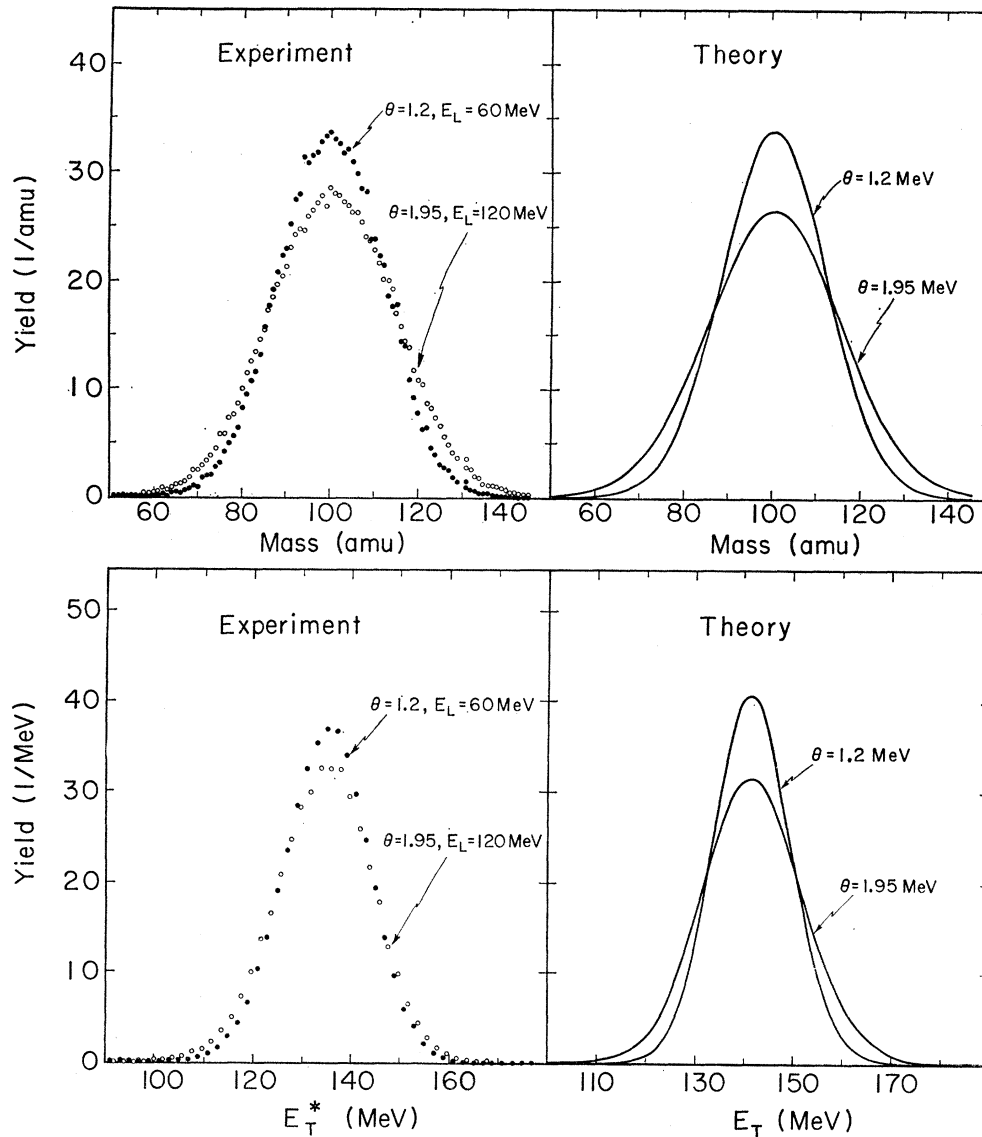
Fig. 5. Theoretical and experimental mass-yield and energy-yield distributions for the fission of Tl^{201} produced by bombardments of Au^{197} with He^4 ions at two different energies. The units of yield are arbitrary, and the E_T^* scale refers to the $\theta = 1.2$-MeV case.

regions of constant probability of finding an event in the theoretical case. The advantage of this presentation is that all available information is included on a single diagram.

For any given combination of projectile and target, the average over-all total kinetic energy is constant, within experimental limits, for all excitation energies studied. For this reason, it was possible to normalize the over-all yield-total kinetic energy distributions shown in Figs. 4–7 in such a way as to make, for any given type of reaction, the over-all $\langle E_T \rangle$ at all values of the nuclear temperature equal to $\langle E_T \rangle$ at the lowest temperature. Such normalization in Figs. 4–7 was necessary to adequately illustrate the effect of temperature on the widths of distributions.

As was discussed earlier, the theoretical expressions which apply to the relatively high nuclear temperatures

encountered in this work are not expected to hold at very low temperatures. For this reason the theoretical curves of Figs. 8 and 10 extend only over the range of temperature which applies to the experiments presented in this work.

V. DISCUSSION

In Sec. II the measurement of two-dimensional density-of-events distributions, which had as coordinates the pulse heights produced by both fission fragments from any given event, have been described. Section III outlined the method by which these distributions have been transformed to mass-total kinetic energy distributions $P(A_1, E_T^*)$. The basic features of the Nix-Swiatecki theory which yields similar distributions from first principles have also been described. In Sec. IV the experimental results have been presented, and in
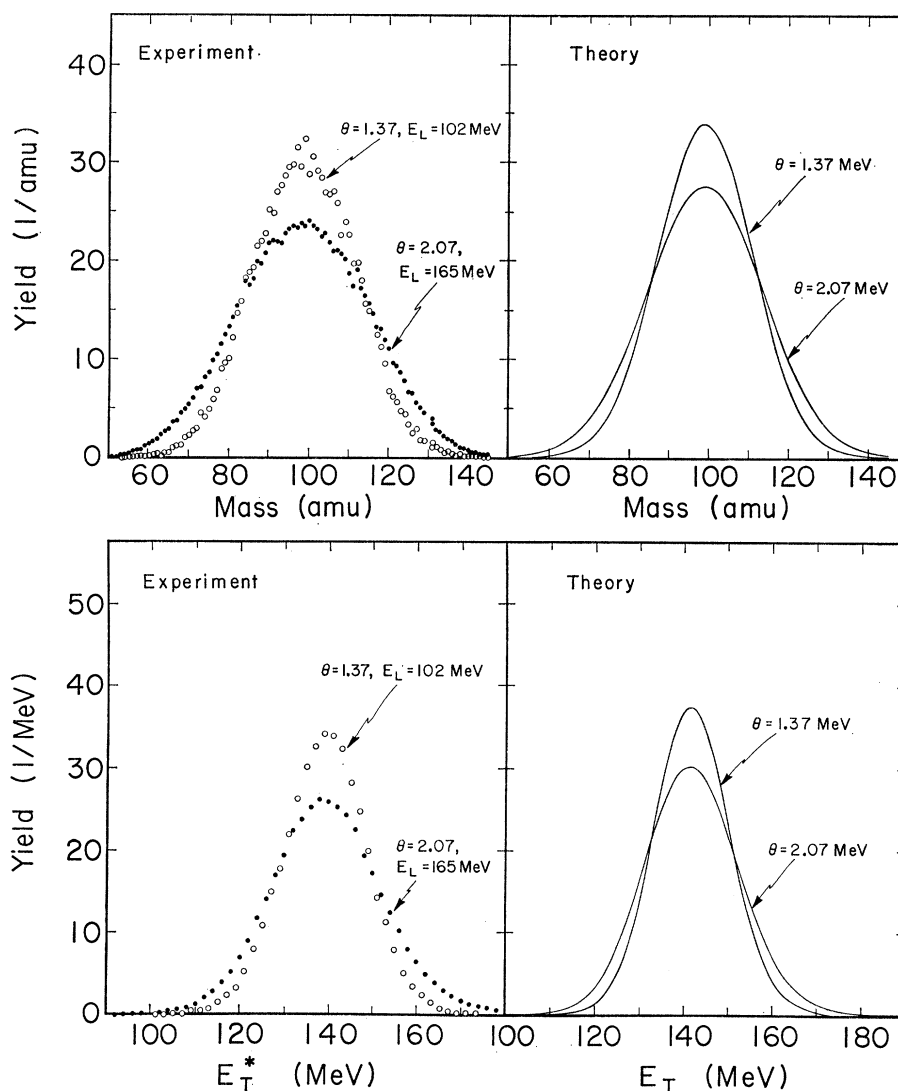
FIG. 6. Theoretical and experimental mass-yield and energy-yield distributions for the fission of Pb^{198} produced by bombardments of W^{182} with O^{16} ions at two different energies. The units of yield are arbitrary, and the E_T^* scale refers to the $\theta = 1.37$-MeV case.

this section the theoretical and experimental distributions will be compared.

A number of important points must be borne in mind during the course of the discussion of results and comparisons with theory. The first of these is the fact that the theory does not include the use of any adjustable parameters. The experimental distributions have not been normalized to the theoretical ones in any way. The size, surface tension, and charge of the idealized liquid drops of Nix and Swiatecki are those which apply to actual nuclei as determined from Green's[22] analysis of ground-state masses. Comparisons with experimental results from the fission of real nuclei do not involve the introduction of new parameters since all other quantities are calculated directly from the model.

The second point concerns the question of angular momentum effects. During the course of a bombard-

ment that involves any particular combination of target, projectile, and bombarding energy, the projectile may strike the target with varying impact parameters. Thus, the angular momentum ranges from zero to some maximum value, which may be as large as 100 units of $\hbar$ in the cases of heavy-ion bombardments. Due to the existence of such angular momentum distributions and the fact that the theory at this stage has not concerned itself with this problem at all, we shall content ourselves with a qualitative discussion of this effect.

The last point to be recalled is the fact that the measured $P(A_1, E_T^*)$ distributions are obtained after the emission of neutrons from the fragments, whereas the theory refers to pre-neutron emission energies. While it is difficult to correct the entire experimental distribution in such a way as to obtain a pre-neutron emission distribution, the correction of the experimental statistical moments, and of the entire theoretical dis-
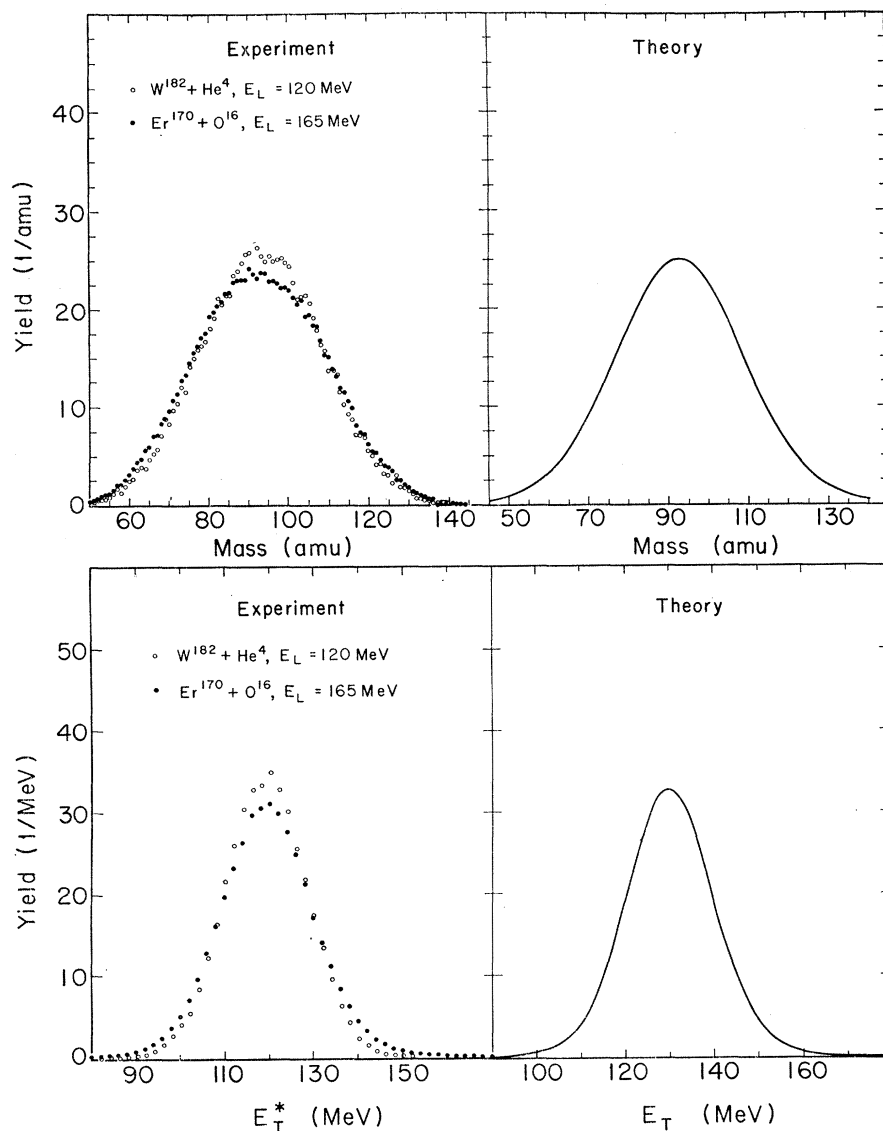
[22] A. E. S. Green, Phys. Rev. **95**, 1006 (1954).

FIG. 7. Theoretical and experimental mass-yield and energy-yield distributions for the fission of Os^{186} at a nuclear temperature of 2 MeV. The Os^{186} compound nucleus was produced by an O^{16} and a He^4 bombardment. The units of yield are arbitrary.

tributions, is somewhat easier. In the first method (Appendix A), however, approximations have to be made in the derivations of the necessary formulas,[6] while the second method (Appendix B), although consistent within the framework of the theory, requires the theory to describe adequately not only the mass and total kinetic energy distributions of interest in this work but also the distributions of excitation energies of the fragments. Thus, both methods must be viewed with some caution. For these reasons, whole distributions shown in Figs. 1 to 3 have not been corrected for neutron effects, while both corrected and uncorrected results are given for the moments of over-all distributions. The moments of conditional distributions are, in general, uncorrected, but the corrected results are not very different from uncorrected results.

The comparisons have been made as a function of the

magnitude of two important variables: (a) the temperature of the compound nucleus in its saddle configuration and (b) the angular momentum of the compound nucleus. As was discussed above, the first of these two effects is an essential feature of the theoretical calculations, while the second effect has not been considered by Nix and Swiatecki in the present state of development of their theory.

General agreement between experiment and theory can be found in several features of the distributions, although some areas of agreement are restricted to only a portion of the experimental data. The theoretical prediction of the over-all average total kinetic energy $\langle E_T \rangle$, is very good, and agreement is found for both heavy-ion and He^4 results, as can be seen from Table I. Examination of the contour diagrams reveals that the theory correctly predicts a general triangular appear-

ance of the distributions, although the heavy-ion distributions tend to be elliptical rather than triangular. The shape of theoretical and experimental over-all mass-yield and total kinetic energy-yield curves is similar, and their widths agree, within experimental errors, in about half of the cases studied. Concerning the moments of the conditional distributions presented in Figs. 12 to 17, agreement may be found in the He[4] induced-fission cases, particularly at low bombarding energies.
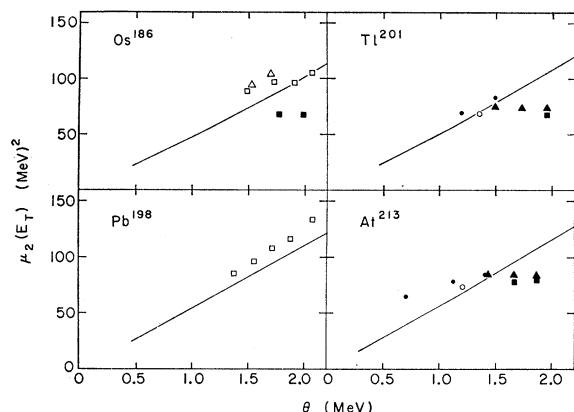

FIG. 8. Variances of the over-all total kinetic energy distributions, $\mu_2(E_T)$, as a function of the nuclear temperature θ, for several compound nuclei. The open triangles in the Os[186] case refer to the reaction $Yb^{174}+C^{12}=Os^{186}$. The open squares refer to $Er^{170}+O^{16}=Os^{186}$, while the closed squares refer to $W^{182}+He^4$ $=Os^{186}$. The Pb[198] was produced by O^{16} bombardments of W^{182}. The Tl[201] and At[213] were obtained by He^4 bombardments of Au^{197} and Bi^{209}, respectively. The different symbols in these two cases represent different experiments. The solid line shows the theoretical result. The experimental points have been corrected for neutron emission effects. The size of the symbols is not to be taken as representative of the errors involved. Estimated errors are tabulated in Table I.
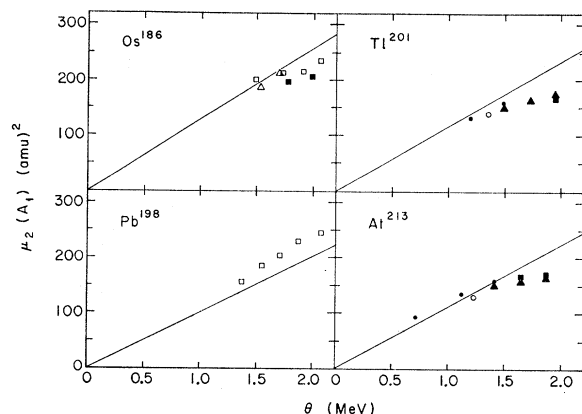

FIG. 9. Variances of the over-all mass-yield distributions, $\mu_2(A_1)$, as a function of the nuclear temperature θ. The symbols have the same meaning as in Fig. 8. The solid line gives the theoretical calculations. The experimental results have been corrected for prompt neutron emission effects. The size of the symbols is not representative of the errors in measurement.
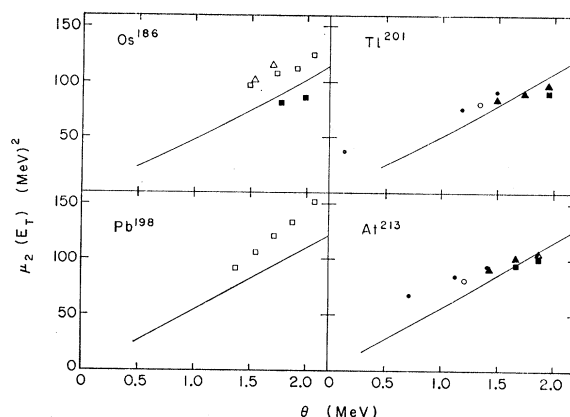

FIG. 10. Variances of the over-all total kinetic energy distributions as a function of the nuclear temperature θ. Identical to Fig. 8, but experimental results have not been corrected for neutron evaporation effects.
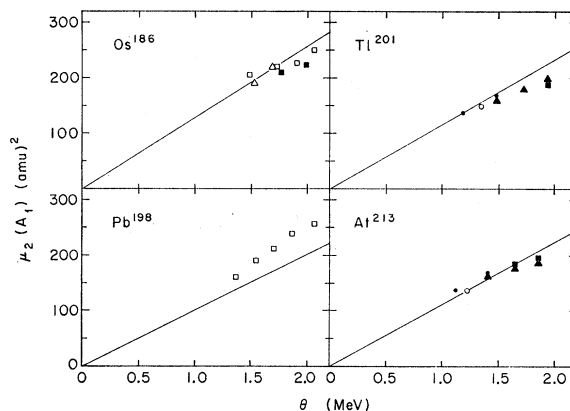

FIG. 11. Variances of the over-all mass-yield distributions as a function of the nuclear temperature θ. Identical to Fig. 9, but experimental results have not been corrected for neutron evaporation effects.

A. Temperature Dependence

The fact that the Nix-Swiatecki theory has not been developed to the point of including angular momentum effects makes it more appropriate to compare the theory with the He[4] data than with the heavy-ion-induced data. For this reason the discussion will initially be restricted to the He[4] data, while the heavy-ion data will be considered separately later.

An examination of the contour diagrams for the fission of At[213] produced by a He[4] bombardment of Bi[209] (Fig. 1) shows that as the temperature increases, both experimental and theoretical distributions broaden, and the triangular shapes of the measured distributions tend to show more rounded corners. It is interesting to note that while the width of the measured distributions increases more slowly than that of the calculated distributions, the discrepancy is greater in the E_T direction than in the mass direction. This point is illustrated
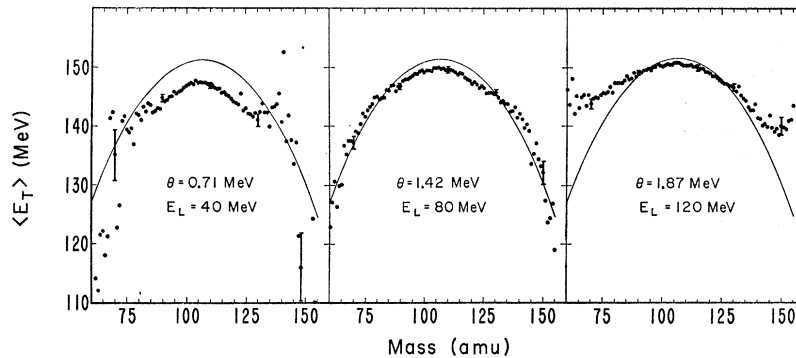
FIG. 12. Average total kinetic energy $\langle E_T \rangle$, as a function of mass for the fission of At^{213}. The solid curves give the theoretical results, the closed circles the experimental results. The experimental results are corrected for neutron evaporation effects.

in Figs. 4 and 5, where the over-all distributions are presented. Thus, for example, in the extreme case there is little difference between the E_T-yield curves from the reaction $Au^{197}+He^4=Tl^{201}$ measured at laboratory energies of 60 or 120 MeV. The differences in width between the mass-yield curves is greater, but not as great as that predicted by theory. Figures 8 to 11, which show the widths of the over-all distributions as a function of temperature provide a summary of the temperature broadening effect. In the He^4-induced cases, the results which are uncorrected for neutron effects (Figs. 10 and 11) provide better agreement between experiment and theory than those which are corrected for neutron effects (Figs. 8 and 9). While the method used in these

FIG. 13. Average total kinetic energy $\langle E_T \rangle$, as a function of fragment mass for the cases of $W^{182}+O^{16}=Pb^{198}$ (at two bombarding energies), $W^{182}+He^4=Os^{186}$ and $Er^{170}+O^{16}=Os^{186}$. The solid curves give the theoretical results. The closed circles give experimental results corrected for neutron evaporation effects.

corrections does include approximations, the direction of the effect, i.e., a broadening of measured distributions due to prompt neutron emission, is nevertheless correct. Thus it does not appear possible to explain the discrepancy by uncertainties in the neutron corrections. The widths of mass distributions in these He^4 bombardments broaden as predicted up to about 80-MeV bombarding energy. Beyond this energy the width does not increase with temperature as rapidly as predicted. For the same reactions the widths of the over-all E_T distributions as a function of temperature present an even greater problem. They are too large at low temperatures and too low at high temperatures. In the $Au^{197}+He^4$ case, for example, the plot of the experimental variance of E_T versus θ is, in fact, virtually flat.

The "washing out" of the triangular distribution shape has been pointed out in Fig. 1. This effect is also present in Figs. 14 and 16, which give the widths of conditional distributions for the $Bi^{209}+He^4$ case. The tendency of the $\langle E_T \rangle$-versus-mass curves of Fig. 12 to flatten with increasing nuclear temperature should also be noted. If these effects were merely due to poor experimental resolution, it would be expected that they would be more prominent in the distributions measured at lower bombarding energies, because of the more difficult experimental conditions which result from lower cross sections. The experimental results show just the reverse trend to hold.

It must be remembered that as bombarding energy increases, not only the temperature but also the average angular momentum increases. As will be discussed later, some of the effects due to angular momentum tend to be similar to those due to high temperatures. It is therefore difficult to separate one cause from the other as far as the "washing out" of the triangular distributions is concerned. The general conclusion of the above discussion, namely, that the widths of the measured distributions do not appear to increase as fast with nuclear temperature as predicted by the theory, is, however, independent of any angular momentum considerations since larger angular momenta tend to broaden distributions.

Before the lack of agreement in temperature-dependent features is assigned to shortcomings of the theory,
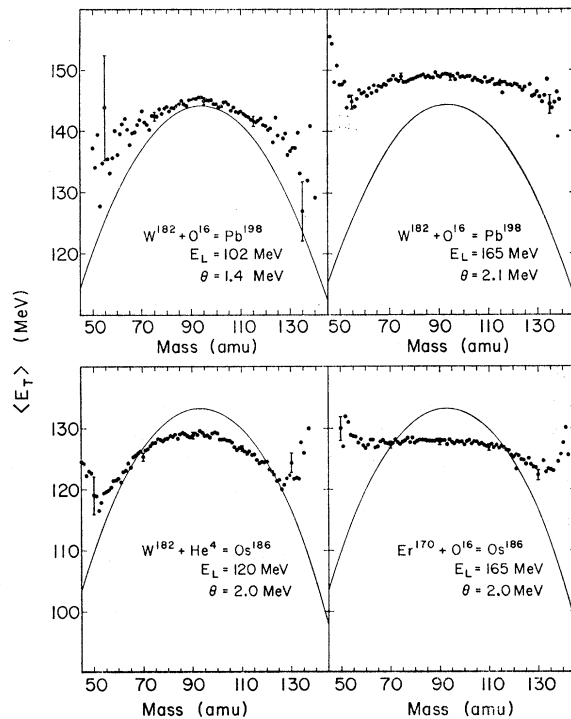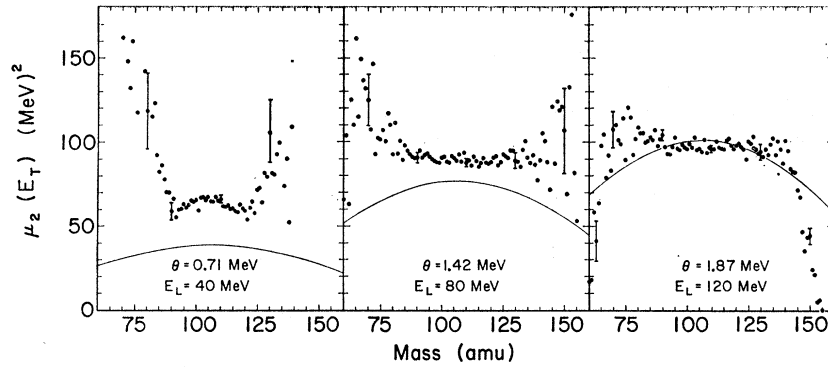
FIG. 14. Variances of the conditional total kinetic energy distributions, $\mu_2(E_T)$, as a function of mass for the case of the fission of At^{213}. The solid lines give the theoretical results; the closed circles give experimental results not corrected for neutron effects.

several possible contributing causes should be examined. These all depend in one way or another on uncertainties in the nuclear temperature. The first problem could be that the equation of state that we have chosen to relate θ to the excitation energy might not apply in some regions of this study. The evidence that shows that this is not likely to be the only explanation is the fact that almost no change in the widths of experimental E_T-yield curves is observed in the He^4 bombardments ranging from bombarding energies of 80 MeV to energies of 120 MeV. This would imply that the expression for θ is independent of excitation energy in this region. It
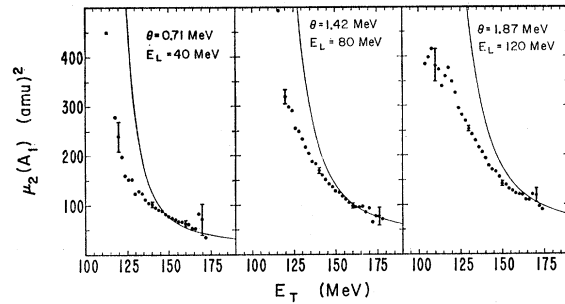

FIG. 16. Variances of conditional mass distributions, $\mu_2(A_1)$, as a function of the total kinetic energy, E_T, for the case of $He^4 + Bi^{209} = At^{213} \rightarrow$ fission. The solid curves give theoretical results. The closed circles give experimental results not corrected for prompt neutron evaporation effects.
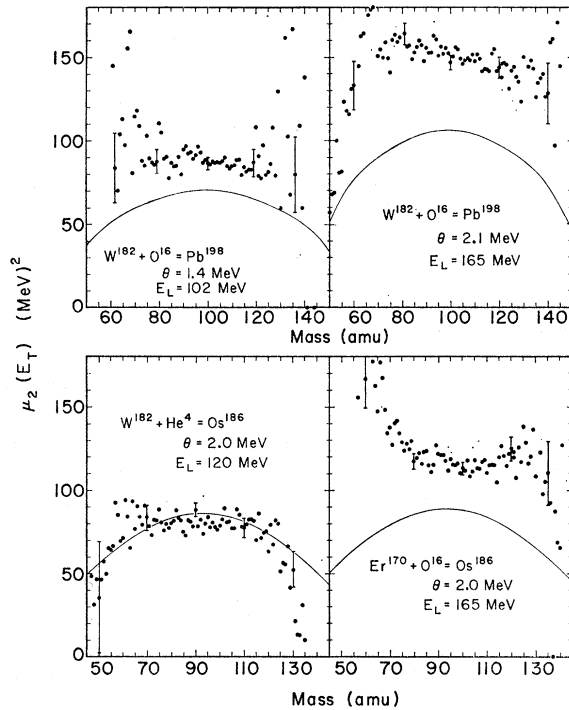

FIG. 15. Variances of the conditional total kinetic energy distributions, $\mu_2(E_T)$, as a function of mass for the cases of the fission of Pb^{198} and Os^{186}. The solid lines give the theoretical calculations. The closed circles give experimental results not corrected for neutron effects.
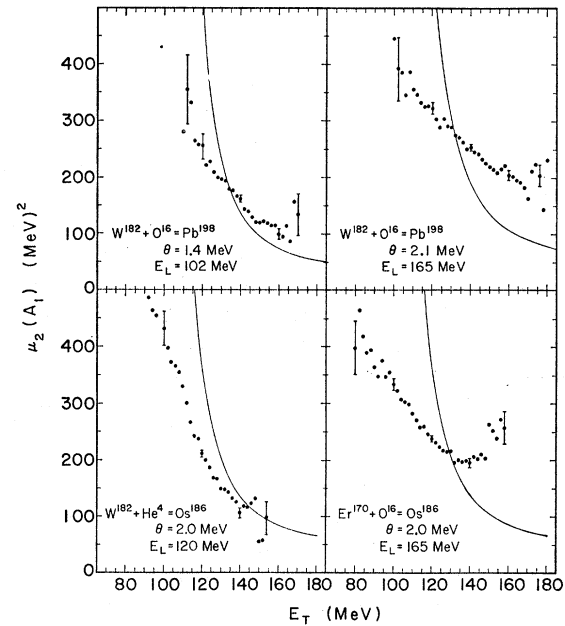

FIG. 17. Variances of conditional mass distributions, $\mu_2(A_1)$, as a function of the total kinetic energy, E_T, for the cases of the compound nuclei Pb^{198} and Os^{186}. The solid curves give theoretical results, and the closed circles give experimental results not corrected for neutron evaporation effects.

should be noted, however, from a comparison of Fig. 8 with Fig. 10, that experimental over-all widths are completely independent of temperature only after corrections for neutron emission from fragments are made, and thus the above conclusion relies to some extent on the accuracy of these corrections. The next possibility is a large contribution at high He^4 energies from fission following direct interactions. Excited nuclei created in this manner do not all possess all of the energy and momentum of the projectile, causing the temperature to be lower than calculated. The distribution widths at high energies would, therefore, be lower than expected, as is indeed the case. The possibility that this effect is a contributing factor was eliminated by a careful angular correlation study for the case of Bi^{209} and 120-MeV He^4 ions, using the method of Sikkeland, Haines, and Viola.[23] No evidence of fission following incomplete momentum transfer was found. A further possibility is that at high energies a considerable number of neutrons is evaporated from the compound nucleus prior to fission, thus reducing its temperature. The measurement and analysis of the fission excitation function of Tl^{201} provided us with level density parameters and the fission barrier for this case.[24] Using these values we extended the calculations of Ref. 24 to high energies and included effects of de-excitation through a neutron evaporation chain by the method described in Ref. 7 and discussed above in Sec. III. It was found that the number of neutrons emitted prior to fission was not large (of the order of one). The calculated fission cross sections, compared with measured cross sections, however, no longer agreed at these high temperatures, regardless of whether neutron evaporation effects were included or not. This made the analysis inconclusive, and the possibility of a large amount of neutron evaporation prior to fission cannot be ruled out. A study of angular distributions at high energies, which could yield independent determinations of θ at the time of fission, would be of interest.

The following summary describes the situation of the temperature dependence of distribution widths. A discrepancy between experiment and theory does appear to exist, particularly in the case of the widths of over-all total kinetic energy-yield distributions. There are, however, a number of possible effects which contribute to errors in the evaluation of the nuclear temperature. These could conceivably combine with errors in the corrections for neutron emission from the fragments to cause a large portion of the observed disagreement. Our analysis of these effects, however, indicates them not to be large enough to eliminate the discrepancies, although this analysis does not constitute a conclusive proof. The theory, therefore, seems to predict a too

rapid temperature dependence, but the exact extent of this discrepancy cannot, at present, be determined.

From an examination of Fig. 6, where the $W^{182}+O^{16}$ reaction is presented, and from the heavy ion data in Figs. 8–11, there appears to be little disagreement between experiment and theory as far as the temperature dependence is concerned. This agreement, however, is probably fortuitous in that it may be caused by the broadening effects of angular momentum, which are described in the next subsection.

B. Angular-Momentum Effects

The two reactions $W^{182}+He^4=Os^{186}$ and $Er^{170}+O^{16}=Os^{186}$ are particularly useful in determining the effect of angular momentum on the measured distribution. Using O^{16} ions of 165-MeV energy and He^4 ions of 120 MeV, the nuclear temperature at the saddle is approximately equal (2 MeV), and any differences in the observed distributions should be entirely due to different amounts of angular momentum. For W^{182} bombarded with 120-MeV He^4 ions, the average angular momentum is estimated to be about 30 units of $\hbar$, while for Er^{170} and 165-MeV O^{16} ions, it is of the order of 70 units of $\hbar$. As can be seen from Fig. 3, there are noticeable differences in the distributions. The He^4-induced reaction gives results that resemble the triangular theoretical distribution more than the almost oval O^{16} induced distribution. This difference may also be seen on examining the moments of conditional distributions (Figs. 13, 15, and 17) which are sensitive to the general shape of the distributions. In all cases the He^4 bombardment produces results that agree better with theory than the O^{16} bombardment. The conclusion is that qualitatively angular momentum is responsible for a general "washing out" of the predicted triangular shape of the distribution. It is also responsible for a broadening of the distribution, as can be seen from Fig. 7 and even more readily from Table I. The possibility that the differences between the two distributions are due to errors in measurements appears very unlikely. It can be seen from Table I that the differences in values of the over-all widths are well outside experimental errors. The estimate of these errors was discussed in Sec. IV. One further possible source of error, restricted to the case of heavy-ion reactions and mentioned in Sec. II, is the loss of energy resolution with increases in beam intensity. The contribution from this effect was made insignificant by making measurements at several values of beam intensity, extrapolating energy widths to zero-beam intensity and choosing a beam level for other runs (about 20 mμA) at which energy widths differed very little (less than $\sim 1\%$ in the variance of the distribution) from those at zero-beam intensity.

The effects of angular momentum examined above are confirmed by comparing the reaction $W^{182}+O^{16}=Pb^{198}$ with the reaction $Bi^{209}+He^4=At^{213}$. The two compound nuclei have almost identical values of the fissionability

[23] T. Sikkeland, E. L. Haines, and V. E. Viola, Jr., Phys. Rev. **125**, 1350 (1962).

[24] D. S. Burnett, R. C. Gatti, F. Plasil, P. B. Price, W. J. Swiatecki, and S. G. Thompson, Phys. Rev. **134**, B952 (1964).

parameter,[25] and the ranges of temperature involved are also similar. Comparison of Figs. 1 and 2, however, shows the Bi distributions to resemble their theoretical counterparts more than the equivalent W distributions. This is again reflected in the curves of first and second moments (Figs. 13, 15, and 17 compared with Figs. 12, 14, and 16). Furthermore, in the 102-MeV O^{16} and W^{182} case, the measured distribution compares fairly well with the theoretical one, while in the 165-MeV bombarding energy case, the comparison is poorer in all aspects. This difference is very likely due to the angular momentum involved, since it is much less significant over a comparable span of nuclear temperature in the He^4-induced fission case.

Although angular-momentum effects are much larger for the heavy ion bombardments, the average angular momentum involved in the case of bombardments with high energy He^4 ions is still quite appreciable (between 25 and 30 units of $\hbar$ at 120 MeV). Since angular momentum has been shown above to change the shapes of measured distributions, similar changes could be present in the case of high-energy He^4 bombardments. The difference in the average angular momentum between the 60 MeV and the 120-MeV He^4 bombardment of Bi^{209}, however, is only about 9 units of $\hbar$, whereas the difference between the 102-MeV and the 165-MeV O^{16} bombardments of W^{182} is of the order of 26 units of $\hbar$ for a comparable range (about 60 MeV) of bombarding energy. For this reason we have neglected angular momentum in the discussion of the He^4 results up to now. It should be stressed, nevertheless, that there are no reliable criteria for estimating whether or not angular momentum contributes significantly to the observed changes in the distributions as the bombarding energy is increased. It has also been shown above that angular momentum effects tend to broaden the observed distributions. The widths of the experimental He^4-induced distributions are, however, already too narrow at high energies when compared with their theoretical counterparts. Thus any angular momentum effects would strengthen the conclusion of the last subsection that the theoretical temperature dependence of the widths of the over-all distributions is too rapid.

As was mentioned earlier, the theory of Nix and Swiatecki is expected to apply to the fission of elements lighter than radium (i.e., to cases for which the fissionability parameter, x is $\lesssim 0.68$). One of the reasons for this restriction is that above $x \simeq 0.68$ the saddle-point shape no longer consists of two well-defined fragments connected by a relatively thin neck, and thus cannot

be approximated by two tangent spheroids.[1] As angular momentum increases, recent liquid-drop calculations indicate[18] that the neck grows thicker. Even at lower values of x, the data may be outside the range required for comparisons with theory because of the presence of a thick neck produced by large angular momentum. Reference 18 gives quantitative results on the increase in thickness of the neck with angular momentum. It was found that for the maximum angular momenta involved in the $Er^{170}+O^{16}$ bombardment the neck was no thicker than that involved in the low energy $Bi^{209}+He^4$ bombardments, in which agreements between experiment and theory were excellent. Thus this effect of saddle-point neck thickening may possibly play a role, but does not in itself explain all angular momentum effects.

VI. SUMMARY AND CONCLUSION

To summarize the comparisons presented above, the following factors should be pointed out:

(1). In cases involving low angular momenta and low nuclear temperatures, the agreement between experiment and theory is excellent. An examination of the distribution resulting from the 80-MeV He^4 bombardment of Bi^{209} in all its aspects illustrates this point. The theoretical distribution is a very good replica of the experimental distribution in every way.

(2). The dependence on temperature of the widths of distributions is different from that predicted by the theory. This lack of agreement may be due in part to errors in the calculation of nuclear temperatures. In the heavy-ion cases, where agreement in temperature dependence is found, such agreement is likely to be fortuitous.

(3). Angular-momentum effects, which have not been included in the theoretical development, tend to broaden the experimental $P(E_T^*,A_1)$ distributions, and cause their contour representations to lose the predicted triangular shape.

To conclude, it must be stressed that the general agreement between theory and experiment is remarkably good, when we remember the restricted model which forms the basis of the theory. Not only does it reproduce reasonably well such gross features as the average total kinetic energy and the widths of mass-yield curves, but it predicts accurately the general triangular shape of the complete mass-total kinetic energy distributions. The only possibly serious shortcoming of the theory is the prediction concerning the temperature dependence of the widths. Even this problem may be due in part to errors in the evaluation of nuclear temperatures. We, therefore, consider the Nix-Swiatecki theory to be useful in providing a theoretical basis for fission data of elements lighter than radium. The theory does not restrict itself to mass-total kinetic energy distributions, and comparison with other types of data (e.g., excitation energies of fragments as reflected in their neutron emission distributions) would

---

[25] The fissionability parameter x may be defined by: $x = E_c^0/2E_s^0$, where E_c^0 and E_s^0 are the Coulomb and surface energies of a sphere, respectively. This definition is equivalent to the following alternative definition: $x = (Z^2/A)/(Z^2/A)_{crit}$. The value for $(Z^2/A)_{crit}$ of 50.13 is usually found in the literature. Recent experiments (see Ref. 24), however, indicate that a better value for $(Z^2/A)_{crit}$ is 48.4. When comparisons are made with the theory of Nix and Swiatecki,[3] the old value of 50.13 was retained so that the set of nuclear constants used throughout their work and this paper form a self-consistent set.

be extremely useful. It would also be desirable to evolve a similar theory that includes angular momentum effects, and one that is more realistic in adding a hyperbolic neck between the two spheroids when these are overlapping or tangent to each other, as in the case of saddle-point shapes. Preliminary work on this latter problem has been done by Nix and Swiatecki with encouraging results.

ACKNOWLEDGMENTS

APPENDIX A: NEUTRON CORRECTION FORMULAS TO THE MOMENTS OF EXPERIMENTAL CONDITIONAL DISTRIBUTIONS

The method used in deriving neutron-correction formulas to moments of measured distributions was based on the method of Terrell[26] and that of Haines.[5] The final equations differ somewhat from those of Haines primarily because higher order terms, which have a noticeable effect on the results, are retained.

In the following formulas when two subscripts are given, the first refers to the fragment number, the second to the sequential number of the neutron, the evaporation of which we are considering. Thus, for example, E_{1j} and A_{1j} are, respectively, the energy and the mass of fission fragment 1 after the evaporation of the jth neutron (i.e., $A_{1j} = A_1 - j$). Applying vector analysis to the emission of the jth neutron from fragment 1 at an angle θ_{1j} in the center-of-mass system of the moving fragment, the following expression is obtained:

$$E_{1j} = \frac{A_{1j}E_{1j-1}}{A_{1j-1}} + \frac{m\eta_{1j}}{A_{1j}} - 2\left(\frac{m\eta_{1j}E_{1j-1}}{A_{1j-1}}\right)^{1/2} \cos\theta_{1j}, \quad (A1)$$

where η_{1j} and m are the energy and mass of the emitted neutron, respectively. The above expression is a recur-

[26] J. Terrell, Phys. Rev. **127**, 880 (1962).

sion relation which relates fragment energy before neutron emission to that after neutron emission.

Several assumptions had to be made during the course of the derivations. It was assumed that the neutrons were emitted isotropically. This implies the following relationships: $\langle\cos\theta_j\rangle = 0$ and $\langle\cos^2\theta_j\rangle = \frac{1}{3}$. It was also assumed that no correlation between fragment energy, neutron kinetic energy, and an angle exists, i.e., $\langle E_1\eta\rangle = \langle E_1\rangle\langle\eta\rangle$. Since no information on the average number of neutrons, ν_1, emitted from fragment 1, as a function of E_T and A_1 is available for the reactions studied, the assumption was made that ν_1 is equal to half the total number of neutrons, ν_T, emitted from both fragments during the fission event, averaged over all masses and total kinetic energies, i.e., $\nu_1 = \nu_2 = \nu_T/2 = \nu$.

Correction to the Averages of Conditional Distributions in Kinetic Energy

The correction to the average total kinetic energy for a given mass is obtained by successive application of expression (A1). Neglecting terms of the order of m/A_1 and reducing, the following equation was obtained:

$$\langle E_T^*\rangle = \frac{A_{1\nu}}{A_1}\langle E_1\rangle + \frac{A_{2\nu}}{A_2}\langle E_2\rangle = \langle E_T\rangle\left(1 - \frac{\nu A_2}{A_1 A_c} - \frac{\nu A_1}{A_2 A_c}\right);$$

A_c is the mass of the compound nucleus, and the asterisk here, as in the main text, refers to a quantity uncorrected for neutron effects. Solving for $\langle E_T\rangle$, we obtain the required correction to average total kinetic energy values at fixed values of the mass.

Correction to the Variances of the Conditional Distributions in Total Kinetic Energy

The derivation of corrections to the variance of the conditional total kinetic energy distributions follows a similar pattern and is also based on the successive application of recursion relation (A1). In this derivation, terms of order m/A_c are retained, while higher order terms are not. Thus, recalling the definition of a variance,

$$\mu_2(E_T^*) = \langle E_T^{*2}\rangle - \langle E_T^*\rangle^2,$$

and the relationships,

$$E_T^* = E_{1\nu} + E_{2\nu},$$

and

$$\langle E_T^*\rangle = \langle E_{1\nu}\rangle + \langle E_{2\nu}\rangle,$$

we obtain

$$\mu_2(E_T^*) = \mu_2(E_{1\nu}) + \mu_2(E_{2\nu}) + 2\{\langle E_{1\nu}E_{2\nu}\rangle - \langle E_{1\nu}\rangle\langle E_{2\nu}\rangle\}.$$

It can be shown that, with proper use of expression (A1) and the assumptions discussed above, together with some lengthy but straightforward algebra, evaluating the above expression term by term, the following

equation may be obtained:

$$\mu_2(E_T^*) = \mu_2(E_T)\left(1 - \frac{\nu A_2}{A_1 A_c} - \frac{\nu A_1}{A_2 A_c}\right)^2$$

$$+ \frac{4\nu}{3}\frac{m}{A_c}\langle E_T\rangle\langle\eta\rangle\left[\frac{A_1}{A_2} + \frac{A_2}{A_1}\right] + \text{higher order terms.}$$

The further assumption used in the development of the above equation was that there is no correlation between the kinetic energies of successive neutrons emitted from the same fragment. Solving the above equation for $\mu_2(E_T)$ gives the corrected variance of the E_T distribution at a given mass in terms of the uncorrected variance.

Correction to the Variances of the Conditional Distributions in Mass

The calculation of the correction to the mass-distribution variance for a given total kinetic energy is complicated by the manner in which the masses were calculated from the energy data (see main text). In this work measured masses are given by

$$A_2 = E_1^* A_c / E_T^*,$$

from which it can be shown that

$$\mu_2^*(A_1) = (A_c^2/E_T^{*2})\mu_2(E_1^*).$$

Thus, it was necessary to evaluate $\mu_2(E_1^*)$ for constant values of E_T^*. This was done by using the recursion relation (A1) to evaluate E_1^* as a function of E_1. The expression $E_1 = A_2 E_T/A_c$ was then applied, where E_T was given (also through the recursion relation) by

$$E_T \cong E_T^*\left[1 + \frac{\nu A_2}{A_1 A_c} + \frac{\nu A_1}{A_2 A_c} - 2\left(\frac{m\eta_1 A_2}{A_c E_T^* A_1}\right)^{1/2}\sum_{i=1}^{\nu}\cos\theta_{1j}\right.$$

$$\left. - 2\left(\frac{m\eta_2 A_1}{A_c E_T^* A_2}\right)^{1/2}\sum_{j=1}^{\nu}\cos\theta_{2j}\right].$$

Thus a complete expression for E_1^* expressed in terms of required quantities was available, and its variance could be calculated by first calculating $\langle E_1^{*2}\rangle$ and $\langle E_1^*\rangle^2$. Since the mass distributions are symmetric, we have

$$\langle A_1/A_c\rangle = \tfrac{1}{2} \text{ and } \mu_2(A_1) = \langle(A_1/A_c)^2\rangle - \tfrac{1}{4}.$$

Combining this with the above results and performing a considerable amount of algebra, the final expression obtained is

$$\mu_2^*(A_2) = \mu_2(A_2)\left(1 - \frac{4\nu}{A_c}\right) + 2\nu m A_c\frac{\langle\eta\rangle}{E_T^*}.$$

The solution of this equation for $\mu_2(A_2)$ gives the required corrected expression in terms of the measured uncorrected variance. The further assumption made in this last derivation was that there is no correlation between angles of emission of successive neutrons.

The value of ν (the average number of neutrons evaporated from a fragment) which was required in the above derivations was estimated by means of the following energy-balance expression:

$$E_x + \langle E_R\rangle = \langle E_T\rangle + \langle E_\gamma\rangle + 2\nu(\langle B_n\rangle + \langle\eta\rangle).$$

In this expression, $\langle E_R\rangle$ is the average energy released during the fission process (averaged over all masses) as calculated from a computer program of Milton,[27] E_x is the total excitation energy of the fissioning compound nucleus (obtained from a knowledge of the bombarding energy and the masses of the nuclei involved), $\langle B_n\rangle$ is the average neutron binding energy (also averaged over all masses and obtained from the program of Milton), and $\langle E_\gamma\rangle$ is the average energy associated with the emission of γ rays from the fragments. Since $\langle E_\gamma\rangle$ is not known for the systems studied in this work, the value for the case of californium of 9 MeV was used.[28] $\langle\eta\rangle$, the average kinetic energy of the neutrons, was calculated from[29]

$$\langle\eta\rangle = \tfrac{4}{3}\langle\text{fragment nuclear temperature}\rangle = \tfrac{4}{3}(8\langle X_1\rangle/A_1)^{1/2},$$

where $\langle X_1\rangle$ is the average fragment excitation energy. For the purpose of these calculations, $\langle X_1\rangle$ was taken to be $\tfrac{1}{2}(\langle E_R\rangle + E_x - \langle E_T\rangle)$.

APPENDIX B: THEORETICAL ENERGY MASS DISTRIBUTIONS WHICH INCLUDE PROMPT NEUTRON EVAPORATION EFFECTS

An alternative method for approaching the problem of prompt neutron emission from fission fragments is to include this effect in the theoretical development and obtain distributions that compare directly with measured distributions in every way except for angular momentum effects. Such an approach was possible because Nix and Swiatecki[3] have obtained expressions not only for mass-kinetic energy distributions, $P(E_T,A_1)$, but also for mass-kinetic energy excitation-energy distributions, $P(E_T,A_1,X_1)$. (X_1 is the excitation energy of fragment 1 associated with the collective vibrations and deformations of the fragment.) These latter distributions are given by Nix and Swiatecki only in the lowest order of approximation, which, however, is satisfactory for the purpose of neutron correction.

The following numerical method was used to transform the initial $P(E_T,A_1)$ distributions to corrected $P(E_T^*,A_1)$ distributions. The theoretical mass-total kinetic energy distribution $P(E_T,A_1)$ was divided into unit areas ΔE_T by ΔA_1, where $\Delta E_T = 2$ MeV and $\Delta A_1 = 1$ amu. $P(E_T,A_1)$ was evaluated at the centers of these unit areas. Thus each unit area was characterized

[27] J. C. D. Milton, Lawrence Radiation Laboratory Report UCRL-9883 Rev., 1962 (unpublished).

[28] H. R. Bowman and S. G. Thompson, in *Proceedings of the Second United Nations International Conference on the Peaceful Uses of Atomic Energy* (United Nations, Geneva, 1958), Paper P/652, Vol. 15.

[29] K. J. LeCouteur, Proc. Phys. Soc. (London) **A65**, 718 (1952).

by a combination of E_T and A_1 values, a statistical weight given by the value of $P(E_T,A_1)$ at the center of it, and by its own probability distribution $P(X_1)$ in the excitation energy of fragment 1. The distribution $P(X_1)$ associated with every unit $\Delta E_T \Delta A_1$ area was calculated from the lowest order expression for $P(E_T,A_1,X_1)$ of Nix and Swiatecki. The probability was evaluated at the centers of differential units of ΔX_1, the size of which was left adjustable so that the whole $P(X_1)$ distribution was adequately described in every case. Thus, unit volumes of dimensions ΔE_T by ΔA_1 by ΔX_1 were considered, each with a characteristic combination of E_T, A_1, and X_1 and a statistical weight obtained from evaluating $P(E_T,A_1)$ and $P(X_1)$ at this combination. It was necessary to evaluate the two probabilities $P(E_T,A_1)$ and $P(X_1)$ separately rather than directly from the $P(E_T,A_1,X_1)$ expression because the accuracy required in the E_T versus A_1 distribution was one of second-order approximation, while the available $P(E_T,A_1,X_1)$ expression is one of first order. By means of energy balance considerations and the theory of Nix and Swiatecki, it is possible to calculate the corresponding X_2 for any given value of X_1. The following equation was then applied:

$$E_X + E_R = H_T + E_T + X_1 + X_2.$$

This relationship balances the total energy available, consisting of E_X, the total excitation energy of the compound nucleus and of E_R, the total energy released in the fission process, against the way in which it is distributed to the fragments (X_1 and X_2 are excitation energies due to collective motions of the fragments and H_T is the total internal excitation energy that the fragments possess). E_X and E_R are both obtained from nuclear mass tables.[21] E_R is a function of A_1 and was calculated by means of a computer program of Milton.[27] The above equation thus gives a value for H_T for any particular unit $\Delta E_T \Delta A_1 \Delta X_1$ volume. H_T and E_T were divided between the two fragments; H_T was divided according to $A_1/A_2 = H_1/H_2$ and E_T according to the momentum conservation relationship $E_1/E_2 = A_2/A_1$. Thus, for any given unit volume, the kinetic energies of both fragments, E_1 and E_2, and the total excitation energies of both fragments X_1 and X_2 (where $X_1 = X_1 + H_1$) are known, and the numbers of neutrons evaporated may be obtained.

For each unit volume, the random evaporation of neutrons from both fragments was now considered. Two recursion relations were used for this purpose. The first relates the excitation energy X_{1j} of fragment 1 after the emission of the jth neutron to that before the neutron emission

$$X_{1j} = X_{1j-1} - \langle B_1(A_1) \rangle - \eta_{1j},$$

where $\langle B_1(A_1) \rangle$ is the average neutron binding energy for fragment 1. $\langle B_1(A_1) \rangle$ is a function of the mass split and is averaged over the fragment charge distribution; it is

calculated by the program of Milton.[27] η_{1j} is the kinetic energy of the jth neutron and is given by[29]

$$\eta_{1j} = 2\left(\frac{8X_{1j-1}}{A_{1j-1}}\right)^{1/2}.$$

The neutron evaporation process for fragment 1 is terminated when the following condition holds:

$$X_{1j-1} < \langle B_1(A_1) \rangle + \eta_{1j}.$$

The second recursion relation is given by Eq. (A1) of Appendix A. It relates the kinetic energy before neutron emission to that after neutron emission for fragment 1. Analogous relationships hold for fragment 2. The assumptions of Appendix A concerning the isotropic emission of neutrons in the center-of-mass system and the absence of correlations between successive neutrons were also made in this method. Thus the value of $\cos\theta_{1j}$ in Eq. (A1) of Appendix A was selected by a random number generator between the limits

$$-1 \leq \cos\theta_{1j} \leq 1.$$

By means of successive application of the above two recursion relations, E_1 and E_2 values of any unit $\Delta E_T \Delta A_1 \Delta X_1$ volume were transformed to post-neutron E_1^* and E_2^* values. These were then treated exactly as the measured energies, giving $E_T^* = E_1^* + E_2^*$ and $A_1 = (E_2^* A_c)/E_T^*$. For any unit volume, this statistical random number process was repeated n times, n being the same for all unit volumes of any particular calculation. As n increased, the statistical accuracy of this method increased. A new distribution, $P(E_T^*,A_1)$, was generated from the above results as follows. Each unit volume contributed n times to this new distribution, and the extent of the contribution of the unit volume was determined by its statistical weight mentioned above. The procedure of using differential volumes, characterized by values of E_T, A_1, and X_1 and by statistical weights due to the distributions $P(E_T,A_1)$ and $P(X_1)$ to give contributions to a probability distribution, $P(E_T^*,A_1)$, which has, as coordinates, only the total kinetic energy and mass, is equivalent to a numerical integration over X_1. The new distribution was normalized to the old distribution.

The accuracy of the calculation was governed by n,

TABLE II. Comparison of the methods of correction for prompt neutron evaporation effects. The data refer to the fission of Os[186] as produced by a He[4] bombardment of W[182] at 120 MeV. The method of data correction is given in Appendix A, while the method of correction of theoretical calculations is given in Appendix B. The description of the moments tabulated is given in the caption of Table I.

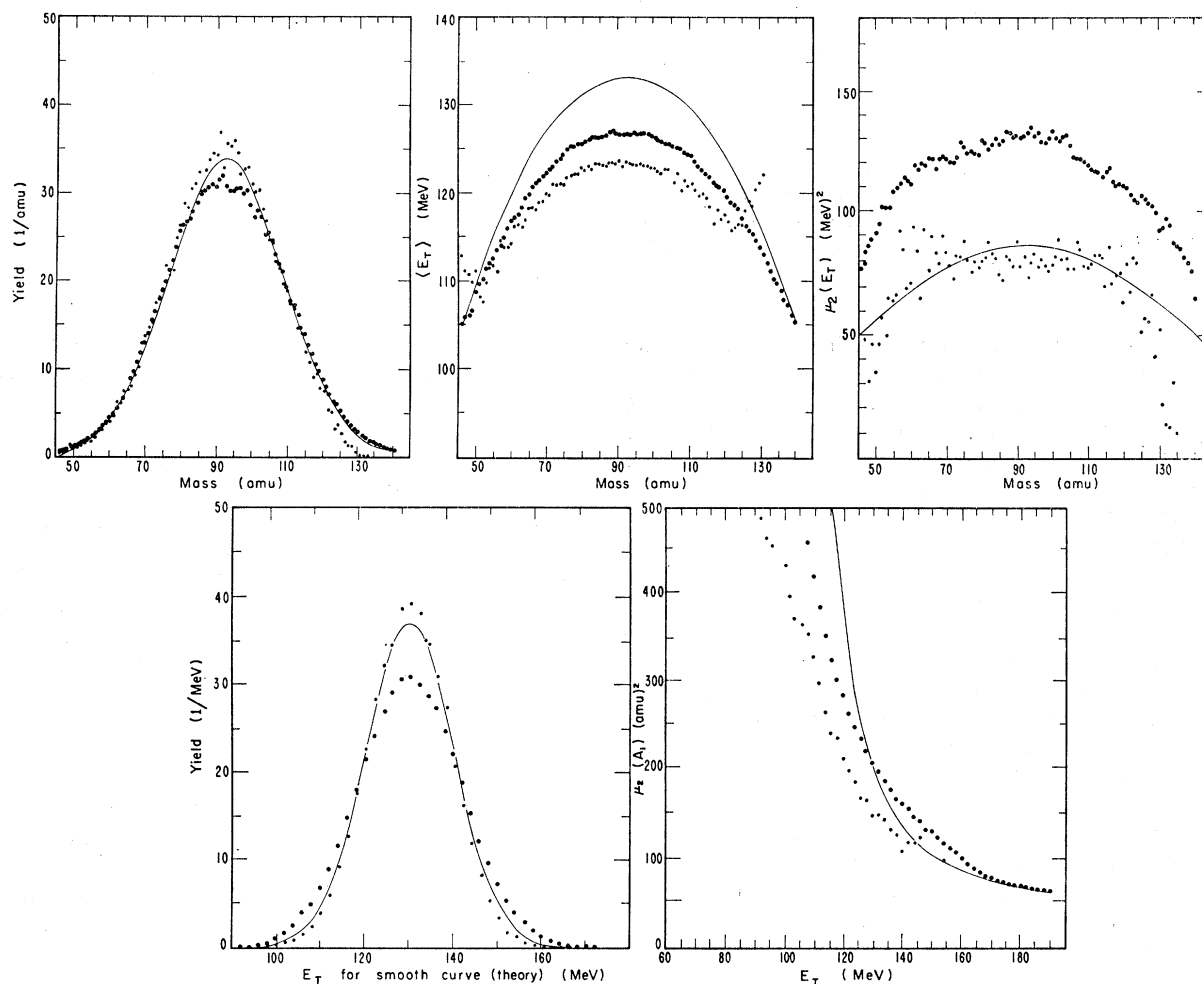|	Experiment uncorrected	Theory corrected	Theory uncorrected	Experiment corrected
$\langle E_T \rangle$ (MeV)	122	124	130	128
$\mu_2(E_T)$ (MeV)^2	86	138	101	68
$\mu_2(A_1)$ (amu)^2	220	278	256	204

FIG. 18. Mass and total kinetic energy-yield distributions and moments of conditional distributions for the reaction $W^{182}+He^4$ $=Os^{186}\rightarrow$ fission at a He^4 energy of 120 MeV. The solid curves give the original theoretical distributions, the larger circles the theoretical distributions which include neutron effects and the smaller circles the experimental distributions not corrected for neutron effects. The labels on the axes and ordinates have the same meaning as those in the corresponding earlier figures that refer to the same reaction, but in which neutron corrections to the theoretical distributions are not included.

the number of times it was repeated for each unit volume, and by the accuracy of the numerical intergration over X_1. Both effects were studied, and reproducibility (for different values of n and different accuracies of the numerical integration) to an accuracy of 0.5% in the moments of the mass-yield and energy-yield distributions was required. The statistical scatter in the yield distributions and in the moments of conditional distributions was greatly reduced as n was increased. The highest value of n used was 20. Higher values were impractical because of the large amount of computer time required. The scatter in the calculated points is greater in the case of moments of the conditional total kinetic energy distributions, taken as a function of mass, than in the case of the moments of conditional mass distributions taken as a function of total kinetic energy. This is in accordance with expectations since the neutron evaporation perturbs the

total kinetic energy much more than it does the mass, when the latter is obtained in the manner described in this work.

Figure 18 shows the results for the reaction of W^{182} with 120-MeV He^4 ($n=20$). It can be seen that, since the experimental distributions were narrower than the uncorrected theoretical ones, the correction due to neutron effects does not help the agreement as far as the width is concerned. The agreement between the shapes of the theoretical and experimental distributions, however, is enhanced by including neutron effects in the theoretical distribution. This is reflected in the cases of the $\mu_2(A_1)$ versus E_T and $\langle E_T\rangle$ versus mass plots and also in the case of $\mu_2(E_T)$ versus mass, if the difference in magnitude is neglected and only the shape of the curve is considered. Table II gives comparative values of moments of the over-all distributions (for the $W^{182}+He^4$ case) for the two methods of neutron correction.